Journal of Organometallic Chemistry 889 (2019) 53–61

Contents lists available at ScienceDirect

Journal of Organometallic Chemistry

journal homepage: www.elsevier.com/locate/jorganchem

New NHC cycloplatinated compounds. Significance of the cyclometalated group on the electronic and emitting properties of bis-cyanide compounds

Sara Fuertes [a], Andrés J. Chueca [a], Antonio Martín [a], Violeta Sicilia [b, *]

[a] Departamento de Química Inorgánica, Facultad de Ciencias, Instituto de Síntesis Química y Catálisis Homogénea (ISQCH), CSIC - Universidad de Zaragoza, Pedro Cerbuna 12, 50009, Zaragoza, Spain

[b] Departamento de Química Inorgánica, Escuela de Ingeniería y Arquitectura de Zaragoza, Instituto de Síntesis Química y Catálisis Homogénea (ISQCH), CSIC - Universidad de Zaragoza, Campus Río Ebro, Edificio Torres Quevedo, 50018, Zaragoza, Spain

ARTICLE INFO

Article history:
Received 18 January 2019
Received in revised form
15 March 2019
Accepted 15 March 2019
Available online 21 March 2019

Keywords:
Cyclometalated NHC
Cyanide
Organometallic compounds
Luminescence

ABSTRACT

Compounds $NBu_4[Pt(C^{\wedge}C^{*A/B/C})(CN)_2]$ ($HC^{\wedge}C^{*A}$ = 1-(4-(ethoxycarbonyl)phenyl)-3-methyl-1*H*-imidazol-2-ylidene **1**, $HC^{\wedge}C^{*B}$ = 1-(4-cyanophenyl)-3-methyl-1*H*-imidazol-2-ylidene **2**, $HC^{\wedge}C^{*C}$ = 1-(3,5-dichlorophenyl)-3-methyl-1*H*-imidazol-2-ylidene **3**) and NBu_4 $[Pt(C^{\wedge}C^{*A/B/C})(^{13}CN)_2]$ (**1′-3′**) were synthesized by addition of KCN (or $K^{13}CN$) to freshly prepared species $[Pt(C^{\wedge}C^{*A/B/C})(NCCH_3)_2]ClO_4$, in a 2:1 M ratio. Single crystal X-ray structures of **1**–**3** showed the absence of intermolecular π-π and Pt-Pt interactions. The $^{195}Pt\{^1H\}$ NMR data of **1**–**3** were obtained and compared with those of the related compounds $NBu_4[Pt(C^{\wedge}N)(CN)_2]$ ($C^{\wedge}N$ = benzoquinolate, bzq; phenylpyridinate, ppy). They indicate that the electronic density on the Pt center is larger for $NBu_4[Pt(C^{\wedge}C^{*A/B/C})(CN)_2]$(**1**–**3**) than for $NBu_4[Pt(C^{\wedge}N)(CN)_2]$, which has been proved through NBO charge distribution analysis. Compounds **1** and **2** resulted to be rather good blue-emitters with their emissions arising mainly from ^{3}IL [π(NHC) → π*(NHC)] excited states with little ^{3}MLCT [5d(Pt) → π*(NHC)] character. The emission of **2** in PMMA film render PLQY (Φ) of 70% and Commission Internationale de L'Eclairage (CIE) coordinates (0.15, 0.19) highly close to the optimal ones for blue emitters (0.15, 0.15).

1. Introduction

Organometallic compounds of Pt(II) containing cyanide as ligand are known since a long time. The cyanide is typically bonded through the C atom; the π-back bonding from the platinum to the cyanide (CN^-) orbitals strengthens the Pt-CN bond and the robustness of the compounds [1,2]. Many of these complexes exhibit very good luminescent properties [3–13] due to the strong field nature of the CN^- ligand, which raises the energy of the corresponding d–d excited state (MC) then precluding fast non radiative deactivation and/or photoreactions. Really well known are the vapochromic and vapoluminescent stacked double complex salts (DCS) $[Pt(CNR)_4][M(CN)_4]$ (M = Pt, Pd; R = alkyl, aryl), reported by Mann and co-workers [14–17]. Experimental work has demonstrated that stronger field and π-acidic ligands, such as CN^- enhance the strength of the Pt···Pt interactions [18–20], as in DCS and in many neutral cyanide complexes such as $[Pt(CNR)_2(CN)_2]$ (R = *i*-C_3H_7 [21], p-C_6H_4-C_2H_5 [22,23], CN^tBu [24]) or $[Pt(CN)_2(N^{\wedge}N)]$($N^{\wedge}N$ = bpy [6,7], i-biq [8,9], phen [10]). When the complexes contain also non bulky π-conjugated systems such as diimines or C,*N*-cyclometalated ligands, π ···· π interactions add to the $Pt^{II}\cdots Pt^{II}$ ones as the major forces to determine the supramolecular structures [9,10,25,26]. As result, square-planar Pt(II) complexes exhibit intense colors and orange-red luminescence due to ^{3}MMLCT (metal-metal-to-ligand charge transfer) $^3[d\sigma^*(Pt)_2 \rightarrow \pi^*(L)]$ and/or $^3\pi\pi^*$ excimeric low-energy excited states in rigid media, which strongly depends on the extent of such interactions [6–10,27,28].

In this field we reported the neutral compounds [Pt(bzq)(CN)(CNR)] [R = ^{t}Bu, Xyl, 2-Np] [4], and the anionic complexes $[Pt(C^{\wedge}N)(CN)_2]^-$ ($C^{\wedge}N$ = benzoquinolate, bzq; phenylpyridinate, ppy) [13]. The later were isolated as the potassium and the tetrabutylammonium salts. The key effect of the counterion on the photophysical properties of these compounds is evident since

* Corresponding author.
E-mail addresses: sicilia@unizar.es, v.sicilia@csic.es (V. Sicilia).

https://doi.org/10.1016/j.jorganchem.2019.03.012
0022-328X/

the water-soluble potassium derivatives $[K(H_2O)][Pt(C^{\wedge}N)(CN)_2]$ ($C^{\wedge}N$ = bzq, ppy) are strongly colored solids. For both, the red (bzq) and purple (ppy) compounds, a prominent absorption, at about 550 nm, and a structureless emission at $\lambda > 700$ nm, are due to ^{1,3}MMLCT [$d\sigma^*(Pt) \rightarrow \pi^*(C^{\wedge}N)$] excited states, typical of linear chain platinum complexes with short Pt···Pt contacts. By contrast, $NBu_4[Pt(C^{\wedge}N)(CN)_2]$ ($C^{\wedge}N$ = bzq, ppy) are yellow solids, not soluble in water, and efficient emitters in the yellowish-green region of the visible spectrum.

Like CN^-, cyclometalated carbenes ($C^{\wedge}C^*$) with two C-σ bonded atoms contribute to enlarge the energy gap between the MC and the emissive excited state of Pt(II) complexes, rendering most often quite efficient blue-phosphorescent compounds [11,29–40]; some of them have been reported by our group [29,30,39]. Our goal in the present work was to bring together cyanide and cyclometalated *N*-heterocyclic carbenes to get efficient blue-emitters. As result, the bis-cyanide compounds $NBu_4[Pt(C^{\wedge}C^{*A/B/C})(CN)_2]$ ($HC^{\wedge}C^{*A}$ = 1-(4-(ethoxycarbonyl)phenyl)-3-methyl-1*H*-imidazol-2-ylidene **1**, $HC^{\wedge}C^{*B}$ = 1-(4-cyanophenyl)-3-methyl-1*H*-imidazol-2-ylidene **2**, $HC^{\wedge}C^{*C}$ = 1-(3,5-dichlorophenyl)-3-methyl-1*H*-imidazol-2-ylidene **3**) were prepared. In each of the three compounds, the metalated aryl group bears electron-withdrawing substituents, which may lead to blue emissions by stabilizing the HOMO. The bulky tetrabutylammonium cation was chosen as counterion, to prevent intermolecular Pt···Pt and π ···· π interactions from happening [11,13]. Then, $NBu_4[Pt(C^{\wedge}C^{*A/B/C})(^{13}CN)_2]$ (**1′**-**3′**) were prepared for a deeper analysis of the $^{13}C\{^1H\}$ NMR data. Comparison of the $^{195}Pt\{^1H\}$ NMR data of **1**–**3** with those of the related compounds $NBu_4[Pt(C^{\wedge}N)(CN)_2]$ together with a NBO charge distribution analysis allowed to prove the high electron donating character of the $C^{\wedge}C^*$ cyclometalated groups. The luminescent behavior of **1**–**3** under UV-light has been also studied and explained on the light of TD and TD-DFT calculations. At the end of our research work, Kato et al. published the closely related compounds $NBu_4[Pt(CN)_2(NHC)]$ (H_2NHC = 1-methyl-3-phenyl-1*H*-imidazolium, 1-methyl-3-phenyl-1*H*-benzimidazolim, 1-methyl-3-(naphthalen-2-yl)-1*H*-imidazolium, 1-methyl-3-(naphthalen-1-yl)-1*H*-imidazolium) [11] which have been taken into account throughout the discussion.

2. Experimental

2.1. Materials and instrumentation

^1H, $^{13}C\{^1H\}$, $^{195}Pt\{^1H\}$ NMR spectra were recorded on a Bruker Avance 400 and 300 MHz instrument using the standard references: tetramethylsilane ($Si(CH_3)_4$) for ^1H and ^{13}C and Na_2PtCl_6 in D_2O for ^{195}Pt. Coupling constant, *J*, is given in Hz and assignments are based on ^1H-^1H COSY and ^1H-^{13}C HSQC and HMBC experiments. Infrared spectra were recorded on Perkin-Elmer Spectrum 100 FT-IR spectrometer (ATR range 250–4000 cm^{-1}) as neat solids. Mass spectra were acquired using the Microflex matrix-assisted laser desorption ionization-time-of-flight (MALDI-TOF) Bruker or an Autoflex III MALDI-TOF Bruker instruments. C, H, and N analyses were carried out in a Perkin-Elmer 2400 CHNS analyzer. UV–visible spectra were registered on a Unicam UV4 spectrophotometer. Diffuse reflectance UV–vis (DRUV) spectra were recorded on a Thermo electron corporation evolution 600 spectrophotometer equipped with a Praying Mantis integrating sphere. The solid samples were homogeneously diluted with silica. The mixtures were placed in a homemade cell equipped with quartz window. Steady-state photoluminescence spectra were recorded on a Jobin-Yvon Horiba Fluorolog FL-3-11 Tau 3 spectrofluorimeter. Phosphorescence lifetimes were recorded with a Fluoromaxphosphorimeter accessory containing a UV xenon flash tube. Nanosecond lifetimes were recorded with a Datastation HUB-B with a nanoLED controller and software DAS6. The nanoLEDs employed for lifetime measurements were of 340 nm. The lifetime data were fitted using the Jobin-Yvon software package and the Origin Pro 8 program. Quantum yields were measured using the Hamamatsu Absolute PL Quantum Yield Measurement System C11347-11. PL films were prepared by drop-casting solutions 5 wt % complex in PMMA (10^{-2}M, CH_2Cl_2) onto a quartz slide and allowing the solvent to evaporate.

2.2. X-ray structure determinations

Single crystals of **1**, **2** and **3** were obtained by slow diffusion of non-anhydrous *n*-hexane (**1**, **3**) or diethyl ether (**2**) into a saturated CH_2Cl_2 (**1**, **3**) or $CHCl_3$ (**2**) solutions of them. The crystal data, data collection parameters, and structure solution and refinement details for the crystal structures determined are summarized in Table 1. Crystals were mounted at the end of quartz fibers. Data collections were carried out on an Oxford Diffraction Xcalibur diffractometer using graphite monochromated MoKα radiation (0.71073 Å). The sample temperature was controlled using an Oxford Diffraction CryojetXL cooling device (100(2) K). The diffraction frames were integrated and corrected from absorption by using the CrysAlis RED program [41]. Structure solution, followed by full-matrix least squares refinement (all data) was performed using SHELX [42] under the WinGX package [43].

All non-hydrogen atoms were refined with anisotropic displacement parameters and refined without positional constraints, except as noted below. The isotropic displacement parameters of all hydrogen atoms were fixed to 1.2 times the *Ueq* value of the atoms they are linked to (1.5 times for methyl groups). In the structure of **1**, some atoms of one of the NBu_4^+ cations are found to be disordered and they were refined with partial occupancy 0.5/0.5 and 0.7/0.3. Constrains in both C-C distances and the thermal ellipsoid parameters were used for these atoms. Because compound **1** exhibits two molecules of complex in the asymmetric unit, a selection of bond distances and angles of the second molecule appears listed in Table S1.

2.3. Computational methods

Density functional calculations were performed using the M06 [44] hybrid density functional under the Gaussian 09 package [45]. The SDD pseudopotential and associated basis set [46] was used for platinum, and the 6-31G* [47,48] basis set was used for all other atoms. Geometry optimizations for S_0 and T_1 states were performed under no symmetry restrictions with the implemented Gaussian 09 package, using initial coordinates of models derived from X-ray data. Atomic coordinates (x, y, z) for the optimized structures of **2** and **3** are collected in the Table S2–S5. ArgusLab and GaussView5 program packages were used for analysis and graphic representation of molecular structures and orbitals. The time-dependent density-functional (TD-DFT) calculations were also carried out in the presence of dichloromethane using the polarizable continuum model (PCM) implemented Gaussian 09 package. Mulliken population analysis was carried out using Gaussian 09 package for interpretation purposes. ArgusLab, Molekel, Gaussum and GaussView5 program packages were used for analysis and graphic representation of molecular structures and orbitals. Atomic charges were calculated by using the NBO analysis option as incorporated in Gaussian 09.

2.4. Synthesis and characterization

$NBu_4[Pt(C^{\wedge}C^{*A})(CN)_2]$ (1). KCN (30.4 mg, 0.46 mmol) was added to a freshly prepared suspension of $[Pt(C^{\wedge}C^{*A})(NCCH_3)_2]ClO_4$

Table 1
Crystallographic data.

	1·CH_2Cl_2	2·$CHCl_3$	3·0.5H_2O
Empirical formula	$C_{32}H_{51}Cl_2N_5O_2Pt$	$C_{30}H_{45}Cl_3N_6Pt$	$C_{28}H_{44}Cl_2N_5O_{0.5}Pt$
Formula weight	803.77	791.16	724.67
Crystalsystem	Monoclinic	Orthorhombic	Monoclinic
Spacegroup	Pc	P*bca*	I2/a
a (Å)	24.5108(5)	15.4030(3)	18.4090(3)
b (Å)	8.54330(10)	18.2893(3)	8.4464(2)
c (Å)	17.3845(4)	24.2617(5)	40.5114(7)
α (°)	90	90	90
β (°)	104.323(2)	90	102.112(2)
γ (°)	90	90	90
Volume (Å)/Z	3527.2(1)/4	6834.8(2)/8	6158.9(2)/8
ρ (Mg/m^3)	1.514	1.538	1.563
μ (Mo-Kα)/mm^{-1}	4.164	4.369	4.757
F(000)	1624	3168	2904
Crystalsize (mm)	0.39 × 0.25 × 0.22	0.42 × 0.25 × 0.15	0.48 × 0.13 × 0.13
Theta range (°)	3.294–30.247	4.21–29.39	4.43–29.37
Reflections collected	30296	30988	52128
Independent reflections [*R*(int)]	16806 [0.0735]	8243 [0.0325]	7689 [0.0463]
Final R_1, wR_2[a] [$I > 2\sigma(I)$]	0.0522, 0.1189	0.0362, 0.0824	0.0343, 0.0839
R_1, wR_2[a] (all data)	0.0759, 0.1246	0.0483, 0.0887	0.0429, 0.0887
Goodness of fit (F^2)[b]	1.015	0.996	1.043
Largest diff. Peak, hole/e.A^{-3}	4.770, −1.566	2.338, −2.074	2.529, −0.982

[a] $R_1 = \Sigma(|F_o|-|F_c|)/\Sigma\,|F_o|$. $wR_2 = [\Sigma w\,(F_o^2-F_c^2)^2/\Sigma w(F_o^2)^2]^{1/2}$.
[b] Goodness-of-fit $= [\Sigma w\,(F_o^2-F_c^2)^2/(n_{obs}-n_{param})]^{1/2}$.

(0.24 mmol) in MeOH (15 mL) at r.t (prepared by reaction of [{Pt(μ-Cl)(C^C*A)}2] (**A**) (110.3 mg, 0.12 mmol) with 2 equivalents of $AgClO_4$ (47.7 mg, 0.23 mmol) in acetonitrile, following previously described methods) [13]. After 2 h the solvent was evaporated to a volume of *c.a.* 5 mL and cooled in the freezer for 10 min. It was then filtered through celite and washed with 2 × 5 mL of cold MeOH (−30 °C). The solution was evaporated to dryness, the residue was suspended in 30 mL of acetone and treated with NBu_4ClO_4 (75.7 mg, 0.22 mmol). After 2 h the solvent was removed under reduced pressure, the residue was then washed with 5 mL H_2O and the solid was filtered and washed with 2 × 5 mL H_2O. After 2 h in the oven (96 °C), the residue was recrystallized from CH_2Cl_2/Et_2O to give **1** as a pure white solid. Yield: 106.7 mg, 67%. Elemental analysis Calcd (%) for $C_{31}H_{49}N_5O_2Pt\cdot 0.5H_2O$: C 51.16, H 6.92, N 9.62; found: C 50.81, H 6.58, N 9.87. IR (ATR, cm^{-1}): ν = 2122, 2111 (m, CN), 1696 (s, CO_2Et). ^1H NMR (400 MHz, CD_2Cl_2) $\delta = 8.74$ (d, $^4J_{H7\text{-}H9} = 1.9$, $^3J_{Pt\text{-}H7} = 55.7$, 1H, H_7), 7.78 (dd, $^3J_{H9\text{-}H10} = 8.1$, 1H, H_9), 7.34 (d, $^3J_{H2\text{-}H3} = 2.0$, 1H, H_2), 7.09 (d, $^3J_{Pt\text{-}H10} = 10.0$, 1H, H_{10}), 6.92 (d, 1H, H_3), 4.36 (q, $^3J_{H\text{-}H} = 7.1$, 2H, CH_2 (OEt)), 4.16 (s, 3H, H_4), 3.28 (m, 8H, CH_2, NBu_4^+), 1.66 (m, 8H, CH_2, NBu_4^+), 1.41 (m, 11H, CH_2, NBu_4^+ and CH_3 (OEt)), 0.99 (t, $^3J_{H\text{-}H} = 7.3$, 12H, CH_3, NBu_4^+). $^{13}C\{^1H\}$ NMR plus HMBC and HSQC (101 MHz, CD_2Cl_2, rt (**1**) 193 K (**1′**)): $\delta = 172.2$ (s, C_1), 167.8 (s, COO), 152.8 (s, C_5), 143.1 (s, C_6), 141.5 (s, $^2J_{Pt\text{-}C7} = 64.8$, C_7), 136.4 (s, $^2J_{C\text{-}C} = 4.6$, $^1J_{Pt\text{-}C} = 840$, $^{13}CN_{trans\text{-}Caryl}$, **1′**), 134.5 (s, $^2J_{Pt\text{-}C} = 1037$, $^{13}CN_{trans\text{-}C^*}$, **1′**), 128.0 (s, C_8), 126.8 (s, C_9), 122.4 (s, $^3J_{Pt\text{-}C3} = 26.4$, C_3), 115.2 (s, $^3J_{Pt\text{-}C2} = 39.1$, C_2), 110.1 (s, $^3J_{Pt\text{-}C10} = 24.9$, C_{10}), 61.0 (s, CH_2 (OEt)), 59.5 (s, CH_2, NBu_4^+), 39.4 (s, C_4), 24.6 (s, CH_2, NBu_4^+), 20.2 (s, CH_2, NBu_4^+), 14.8 (s, CH_3 (OEt))), 14.0 (s, CH_3, NBu_4^+). $^{195}Pt\{^1H\}$ NMR (64.3 MHz, CD_2Cl_2, 293 K): $\delta = -4543.57$. MS (MALDI-): m/z 476.0 $[M]^-$.

NBu_4[Pt(C^C*B)$(CN)_2$](2). Compound **2** was synthesized following the same procedure used for **1** but using **B** (107.3 mg, 0.13 mmol), $AgClO_4$ (53.9 mg, 0.26 mmol), KCN (34.2 mg, 0.52 mmol) and NBu_4ClO_4 (85.2 mg, 0.25 mmol). **2** was obtained as a white solid. Yield: 98.8 mg, 59%. Elemental analysis Calcd (%) for $C_{29}H_{44}N_6Pt$: C 51.85, H 6.60, N 12.51; found: C 51.48, H 6.96, N 12.50. IR (ATR, cm^{-1}): ν = 2218 (m, CN-C^C*), 2121, 2111 (m, CN). ^1H NMR (400 MHz, CD_2Cl_2) $\delta = 8.40$ (d, $^4J_{H7\text{-}H9} = 1.6$, $^3J_{Pt\text{-}H7} = 54.8$, 1H, H_7), 7.37 (dd, $^3J_{H9\text{-}H10} = 8.1$, 1H, H_9), 7.30 (d, $^3J_{H2\text{-}H3} = 2.1$, 1H, H_2), 7.08 (d, $^3J_{Pt\text{-}H10} = 9.8$, 1H, H_{10}), 6.91 (d, 1H, H_3), 4.13 (s, 3H, H_4), 3.24 (m, 8H, CH_2, NBu_4^+), 1.64 (m, 8H, CH_2, NBu_4^+), 1.42 (m, 8H, CH_2, NBu_4^+), 0.98 (t, $^3J_{H\text{-}H} = 7.3$, 12H,CH_3, NBu_4^+). $^{13}C\{^1H\}$ NMR plus HMBC and HSQC (101 MHz, CD_2Cl_2): $\delta = 172.0$ (s, C_1), 152.2 (s, C_5), 144.2 (s, C_6), 143.4 (s, $^2J_{Pt\text{-}C7} = 65.7$, C_7), 135.4 (d, $^2J_{C\text{-}C} = 4.6$, $^1J_{Pt\text{-}C} = 850$, $^{13}CN_{trans\text{-}Caryl}$, **2′**), 133.9 (d, $^1J_{Pt\text{-}C} = 1044$, $^{13}CN_{trans\text{-}C^*}$, **2′**), 129.0 (s, C_9), 122.5 (s, $^3J_{Pt\text{-}C3} = 26.4$, C_3), 120.5 (s, CN-C^C*), 115.1 (s, $^3J_{Pt\text{-}C2} = 37.0$, C_2), 110.5 (s, $^3J_{Pt\text{-}C10} = 24.0$, C_{10}), 109.2 (s, $^3J_{Pt\text{-}C8} = 61.1$, C_8), 59.4 (s, CH_2, NBu_4^+), 39.2 (s, $^3J_{Pt\text{-}C4} = 21.3$, C_4), 24.4 (s, CH_2, NBu_4^+), 20.1 (s, CH_2, NBu_4^+), 13.8 (s, CH_3, NBu_4^+). $^{195}Pt\{^1H\}$ NMR (64.3 MHz, CD_2Cl_2, 293 K): $\delta = -4539.62$. MS (MALDI-): m/z 429.0 $[M]^-$.

NBu_4[Pt(C^C*C)$(CN)_2$] (3). Compound **3** was synthesized following the same procedure used for **1** but using **C** (164.4 mg, 0.18 mmol), $AgClO_4$ (76.7 mg, 0.37 mmol), KCN (47.9 mg, 0.74 mmol) and NBu_4ClO_4 (120.0 mg, 0.35 mmol). **3** was obtained as a white solid. Yield: 118.2 mg, 45%. Elemental analysis Calcd (%) for $C_{28}H_{43}Cl_2N_5Pt\cdot 0.5H_2O$: C 46.41, H 6.12, N 9.66; found: C 46.01, H 6.01, N 9.41. IR (ATR, cm^{-1}): ν = 2125, 2119 (m, CN). ^1H NMR (400 MHz, CD_2Cl_2) $\delta = 7.13$ (d, $^3J_{H2\text{-}H3} = 2.0$, 1H, H_2), 7.03 (d, $^4J_{H\text{-}H} = 1.9$, $^4J_{Pt\text{-}H} = 14.8$, 1H, H_{aryl}), 6.85 (d, $^4J_{H\text{-}H} = 1.9$, 1H, H_{aryl}), 6.77 (d, 1H, H_3), 4.05 (s, 3H, H_4), 3.18 (m, 8H, CH_2, NBu_4^+), 1.57 (m, 8H, CH_2, NBu_4^+), 1.34 (m, 8H, CH_2, NBu_4^+), 0.89 (t, $^3J_{H\text{-}H} = 7.3$, 3H, 12H, CH_3, NBu_4^+). $^{13}C\{^1H\}$ NMR plus HMBC and HSQC (101 MHz, CD_2Cl_2): $\delta = 170.2$ (s, C_1), 151,5 (s, C_{aryl}), 146.54 (s, C_{aryl}), 143.3(s, C_{aryl}), 131.8 (d, $^2J_{C\text{-}C} = 7.1$, $^1J_{Pt\text{-}C} = 1025$, $^{13}CN_{trans\text{-}C^*}$, **3′**), 130.7 (d, $^1J_{Pt\text{-}C} = 892$, $^{13}CN_{trans\text{-}Caryl}$, **3′**), 130.2 (s, C_{aryl}), 126.4 (s, $^3J_{Pt\text{-}C} = 27.7$, C_{aryl}), 122.9 (s, $^3J_{Pt\text{-}C3} = 27.0$, C_3), 115.0 (s, $^3J_{Pt\text{-}C2} = 35.4$, C_2), 109.9 (s, $^3J_{Pt\text{-}C} = 25.0$, C_{aryl}), 59.5 (s, CH_2, NBu_4^+), 39.7 (s,$^3J_{Pt\text{-}C4} = 20.9$, C_4), 24.6 (s, CH_2, NBu_4^+), 20.3 (s, CH_2, NBu_4^+), 14.0 (s, CH_3, NBu_4^+). $^{195}Pt\{^1H\}$ NMR (64.3 MHz, CD_2Cl_2, 293 K): $\delta = -4498.50$. MS (MALDI-): m/z 472.8 $[M]^-$.

3. Results and discussion

*3.1. Synthesis and characterization of compounds NBu_4 [Pt(C^C*A/B/C)$(CN)_2$]*

KCN was added to a freshly prepared suspension of [Pt(C^C*A/B/C)$(NCCH_3)_2$]ClO_4, in a 2:1 M ratio (see Scheme 1 paths a and b).

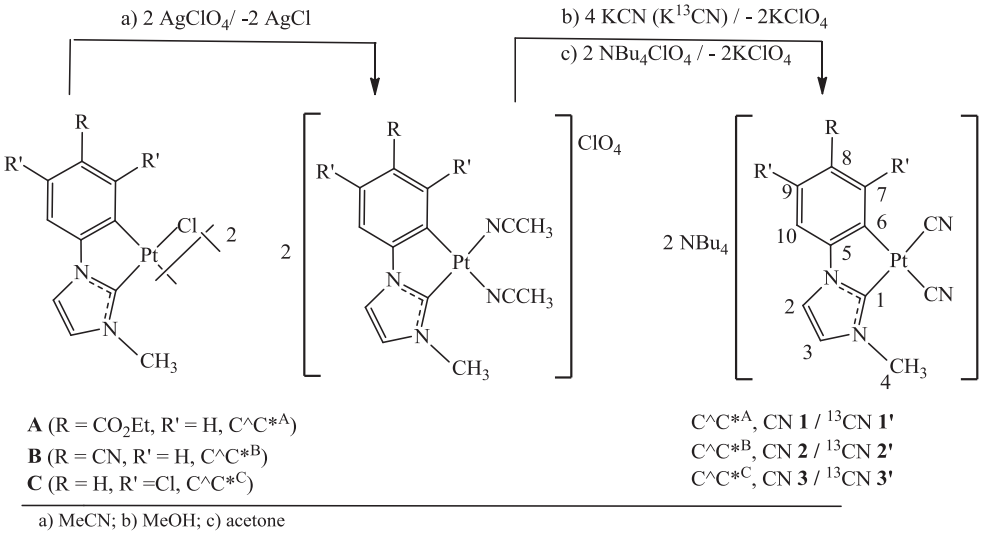

Scheme 1. Synthetic route for compounds **1**–**3**.

After 2 h of reaction, the exchange of the cation was accomplished by reaction of the residue with 1 equiv. of NBu_4ClO_4 in acetone (see Scheme 1 path c). The work-up of the reactions and the subsequent recrystallization of the solids afforded the corresponding compounds $NBu_4[Pt(C^{\wedge}C^{*A/B/C})(CN)_2]$ ($C^{\wedge}C^{*A}$ **1**, $C^{\wedge}C^{*B}$ **2**, $C^{\wedge}C^{*C}$ **3**) as pure solids in good yields (45–67%).

These compounds were fully characterized through different techniques (see Experimental Section and SI). Two absorptions in the range of 2125–2107 cm^{-1} were observed in the IR spectra of compounds **1**–**3**, as expected from the *cis* configuration of two inequivalent cyanide ligands [13,49]. Compound **1** presents an additional absorption at 1696 cm^{-1} attributed to the (C=O) bond in the ethoxycarbonyl fragment [29], while the nitrile group in **2** is responsible of an absorption band at 2218 cm^{-1} [50]. The ^1H NMR spectra of **1**–**3**, showing the expected resonances for the NHC moiety and the NBu_4^+ cation with intensity ratio according to their stoichiometry and the $^{195}Pt\{^1H\}$ NMR spectra (see Fig. S4), showing a singlet at *ca.* −4500 ppm, confirmed the purity of these compounds.

X-ray diffraction studies on a single-crystal of each, **1**, **2** and **3** show mononuclear anionic complexes, in which the Pt atom exhibits a distorted square-planar environment due to the small bite angle of the cyclometalated ligand [C(1)-Pt-C(6) angle of *ca.* 79°] (Fig. 1, Table 2 and S1).

Bond distances and angles in the Pt($C^{\wedge}C^*$) metallacycle are similar to those found in other cyclometalated NHC complexes [11,12,30,50,51]. The Pt-C and C-N bond lengths of the two CN ligands, are similar one to another, as expected from the not much different trans influence of the two carbon atoms of the $C^{\wedge}C^*$ ligand [50]. They are also similar to those observed in other bis-cyanide complexes [3,49].

The complex anions of both, **1** and **2** adopt a zig-zag arrangement in a layer, with the NBu_4^+ cations intercalated between each two layers, thus avoiding π···π and Pt···Pt interactions among them (see Fig. 2). In compound **3**, the presence of water molecules from the crystallization solvent allow the formation of hydrogen interactions between one molecule of water and four complex anions through two O-H···NC (ca. 2.2 Å) and two C-H···O interactions (ca. 2.4 Å) (see Fig. 3 a). On the other hand, the chlorine atoms in the phenyl ring allow the molecules to arrange themselves

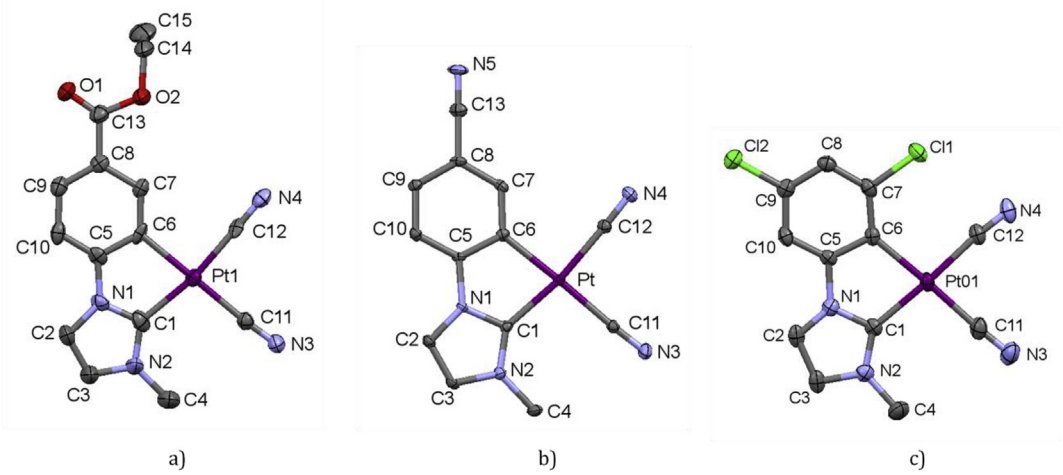

Fig. 1. Molecular structure of the anion in compounds **1** (a), **2** (b) and **3** (c). Thermal ellipsoids are drawn at the 50% probability level. Hydrogen atoms, NBu_4^+ cations and solvent molecules have been omitted for clarity.

Table 2
Selected bond lengths (Å) and angles (°) for **1**–**3**.

	1·CH_2Cl_2[a]	2·$CHCl_3$	3·0.5H_2O
Pt-C(1)	2.034(13)	2.010(4)	2.022(4)
Pt-C(6)	2.072(11)	2.043(4)	2.073(4)
Pt-C(11)	2.031(12)	2.013(4)	2.003(5)
Pt-C(12)	1.947(12)	1.992(4)	1.997(4)
C(11)-N(3)	1.147(15)	1.150(6)	1.158(6)
C(12)-N(4)	1.171(15)	1.153(5)	1.139(5)
C(1)-Pt-C(6)	78.8(5)	79.34(16)	79.67(16)
C(1)-Pt-C(11)	100.8(5)	98.54(16)	98.08(18)
C(6)-Pt-C(12)	91.4(5)	92.23(17)	97.79(16)
C(11)-Pt-C(12)	89.0(4)	89.88(17)	84.65(18)
Pt-C(11)-N(3)	176.3(10)	176.0(4)	176.4(5)
Pt-C(12)-N(4)	177.3(11)	177.9(4)	172.4(4)

[a] Compound **1** exhibits two molecules of complex and two molecules of CH_2Cl_2 in the asymmetric unit (see SI, Table S1).

in pairs via C-H···Cl interactions (Fig. 3 b), yielding chains separated by intercalation of the NBu_4^+ counterions, as in **1** and **2**.

3.2. $^{13}C\{^1H\}$ and $^{195}Pt\{^1H\}$ NMR data and discussion

Compounds $NBu_4[Pt(C^{\wedge}C^{*A/B/C})(^{13}CN)_2]$ (**1′**-**3′**) were prepared following the same method than that used for **1**–**3**, but using $K^{13}CN$, in order to get more spectroscopic details about this kind of species. As can be seen in Table 3, the similarity of δPt and δC in compounds **1** and **2** (**1′** and **2′**) confirmed, once again, the rather similar electronic properties of the cyclometalated NHC ligands CO_2Et-C^C* (C^C*A) and *NC*-C^C*(C^C*B).

The $^{13}C\{^1H\}$ NMR spectra of **1′**-**3′** shows two doublets flanked by platinum satellites (see Table 3, Experimental Section and Figs. S1–S3 in SI), as expected for the two inequivalent cyanides. The $^1J_{Pt\text{-}13C}$ values for *trans*-($^{13}CN/C_{aryl}$) are of the same order than those corresponding to *trans*-($^{13}CN/C_{aryl}$) for $[Pt(C^{\wedge}N)(CN)_2]^-$ (C^N = ppy, bzq). The $^1J_{Pt\text{-}13C}$ values for *trans*-($^{13}CN/C^*$) are just a little bigger than those of *trans*-($^{13}CN/C_{aryl}$) but clearly smaller than those of the *trans*-($^{13}CN/N$) in complexes $[Pt(C^{\wedge}N)(CN)_2]^-$ (C^N = ppy, bzq), in agreement with the high trans influence of the carbenic atom [50]. The $^1J_{Pt\text{-}13C}$ values for the *trans*-($^{13}CN/C^*$) in all the three compounds, **1′**-**3′**, undergoes small variations of no more than 19 Hz, while the coupling constant in the *trans*-($^{13}CN/C_{aryl}$) arrangement present greater differences (up to 52 Hz) depending on the substituent at the cyclometalated (aryl) fragment.

Concerning the $^{195}Pt\{^1H\}$ NMR data, it deserves to be mentioned the great upfield shift of the ^{195}Pt resonances of **1**–**3** compared with those of the cyclometalated compounds $NBu_4[Pt(C^{\wedge}N)(CN)_2]$ (C^N = ppy, bzq) (Table 3), suggesting a bigger electronic density on their Pt centers. Additional information on this matter was inferred from the NBO charge distributions analysis on these compounds, which were calculated at the DFT/M06/SDD/6-31G* level of theory in solution of dichloromethane (Table 3). As a result of the four σ-C atoms bonded to the platinum center and the anionic nature of the complexes, the atomic charges on the platinum centers of **2** and **3** present negative values (−0.095 and −0.087), but not the platinum centers of the related anionic derivatives $NBu_4[Pt(C^{\wedge}N)(CN)_2]$ (C^N = ppy, bzq), which still keep a positive atomic charge of ~ +0.03. Nonetheless, this is in accordance with the trend observed for the ^{195}Pt chemical shifts, and can be explained in terms of the bigger donor ability of C^C* with respect to C^N, in part due to the lower electronegativity of the C atom with respect to the N one.

3.3. Optical properties and theoretical calculations of $NBu_4[Pt(C^{\wedge}C^{*A/B/C})(CN)_2]$

Absorption spectra and DFT calculations. Absorption data are summarized in Table 4 and represented in Fig. 4 (left) and Fig. S5 in SI). As can be seen, solutions (10^{-4} M) of all the three compounds **1**–**3** in dichloromethane show strong absorption bands in the high energy (HE) region at λ< 300 nm (ε> $10^4\,M^{-1}\,cm^{-1}$), commonly assigned to singlet intraligand (^{1}IL) transitions of the cyclometalated NHC ligand. They show as well an intense absorption at λ ~320 nm (ε ≈ $10^4\,M^{-1}\,cm^{-1}$) and their lowest-energy one at *ca.* 340 nm (ε ≈ $10^3\,M^{-1}\,cm^{-1}$), with just little blue-shift of the absorption bands of **3** with respect to those of **1** and **2**. As inferred from the similar absorption spectra, **1** and **2** are a new example of the similarities of the electronic features of the cycloplatinated NHC ligands CO_2Et-C^C* (C^C*A) and *NC*-C^C* (C^C*B) [30,52].

In all the three compounds **1**–**3**, the lowest energy absorption obey Beer's Law, suggesting that in each case it corresponds to a transition in the molecular species with no significant aggregation in concentration up to $5\cdot10^{-4}$ M (see Fig. S6 in SI). Besides, the UV–vis spectra of powdery solid samples (Fig. S7) show no significant differences with those observed in dichloromethane solution.

DFT and TD-DFT calculations were carried out in CH_2Cl_2 solution for compounds **2** and **3** (see Fig. 4 (right), Tables 5 and 6, and Tables S2 and S3 in SI). For compound **1** we assumed similar results than for **2**, since the cycloplatinated NHC ligands C^C*A and C^C*B have already demonstrated their similar electronic properties [30,52]. On the one hand, the highest occupied molecular orbitals (HOMOs) are mainly built from π orbitals of the NHC ligand and dπ orbitals of the platinum center in all cases, with a very small contribution of π orbitals of the CN^- ligands (5–6%). On the other hand, the lowest unoccupied molecular orbitals (LUMOs) still show a small contribution of the ancillary ligands (5–9%) but differ from the HOMOs in the distribution of the electronic density between Pt

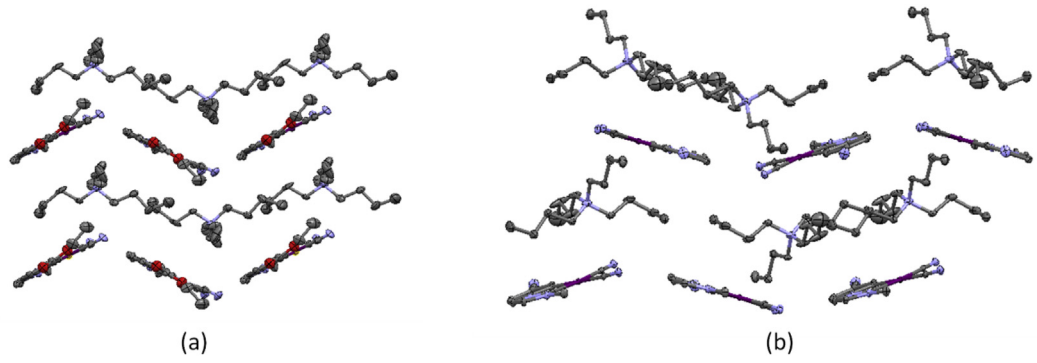

Fig. 2. Molecular packing view of **1** (a) and **2** (b).

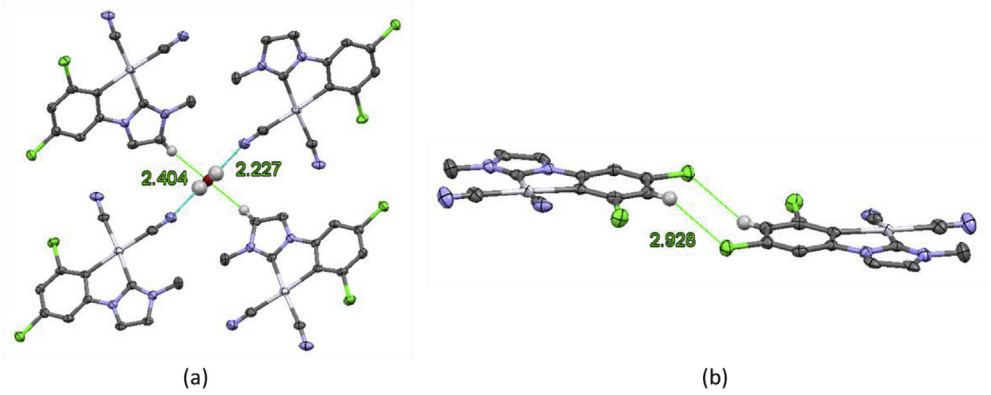

Fig. 3. Intermolecular interactions in the crystal structure of **3**.

Table 3
$^{195}Pt\{^{1}H\}$NMR data (δ(ppm), J(Hz)) in CD_2Cl_2 and calculated NBO charges on the Pt centers.

Compound	δ^{195}Pt	$\delta^{13}CN_{trans\text{-}C^*\ (or\ N)}$ [$^{1}J_{Pt,C}$]	$\delta^{13}CN_{trans\text{-}Caryl}$ [$^{1}J_{Pt,C}$]	NBO charge
$NBu_4[Pt(C^{\wedge}C^{*A})(CN)_2]$ (**1**)[a]	−4543	134.5[1037]	136.4[840]	
$NBu_4[Pt(C^{\wedge}C^{*B})(CN)_2]$ (**2**)	−4539	133.9[1044]	135.4[850]	−0.095
$NBu_4[Pt(C^{\wedge}C^{*C})(CN)_2]$ (**3**)	−4498	131.8[1025]	130.7[892]	−0.087
$NBu_4[Pt(bzq)(CN)_2]$ [49]	−4103	115.8[1424]	144.2[832]	+0.031
$NBu_4[Pt(ppy)(CN)_2]$	−4072	116.7[1418]	145.3[815]	+0.028

[a] Performed at 193K

Table 4
Absorption data in 10^{-4} M solution for compounds **1**–**3** at rt.

Comp	λ abs/nm ($10^3\varepsilon$ $M^{-1}cm^{-1}$)
1	245 (24.0), 252 (28.0), 258 (31.6), 275 (17.0), 293 (10.3), 305 (7.5), 324 (7.7), 342 (3.1) ***CH_2Cl_2***
	240 (16.3), 256 (24.3), 273 (14.6), 290 (7.9), 303 (5.5), 320 (5.8), 338 (2.1) ***MeOH***
	245 (11.6), 252 (13.1), 259 (15.0), 277 (7.0), 294 (4.2), 305 (3.3), 326 (3.3), 344 (1.7) ***THF***
	259, 274, 321 tail to 450 ***Solid***
z	249 (29.1), 255 (32.9), 273 (15.7), 291 (10.9), 304 (7.2), 323 (7.8), 342 (3.3) ***CH_2Cl_2***
	252 (31.9), 270 (15.0), 284 (10.9), 291 (9.2), 302 (6.1), 319 (7.5), 337 (2.7) ***MeOH***
	256 (29.5), 273 (19.5), 291 (13.5), 303 (8.9), 324 (7.1), 330 (5.8), 343 (3.4) ***THF***
	251, 273, 321 tail to 400 ***Solid***
3	246 (19.9), 253 (24.5), 265 (15.3), 286 (8.8), 309 (5.6), 320 (6.5), ***CH_2Cl_2***
	251 (22.6), 264 (18.4), 282 (14.5), 305 (5.3), 317 (4.7) ***MeOH***
	246 (17.9), 252 (21.1), 265 (12.7), 287 (6.9), 293 (6.2), 306 (5.0), 319 (5.6), 326 (5.2), 335 (3.7) ***THF***
	257, 286, 321 tail to 450 ***Solid***

and both halves of the NHC ligand. For both the two compounds, the lowest-energy absorption calculated (S_1) in dichloromethane solution corresponds mainly to the HOMO to LUMO transition (>95%) and therefore, it can be mainly attributed to a ^{1}ILCT [π(NHC) → π*(NHC)] transition but, with some little ^{1}MLCT [5d(Pt) → π*(NHC)] character in **2**.

Emission spectra. At room temperature, compounds **1**–**3** do not display luminescence in CH_2Cl_2 solution under UV light, even in an argon atmosphere, like in other discrete blue-emitting Pt(II) complexes; this kind of compounds show very often low or no emission in fluid solution due to thermal quenching processes via population of higher lying dd* states or exciplexes [11,30,31,35,36,52]. However, in rigid media like CH_2Cl_2 at 77K, solid state (298 K, 77 K) and PMMA films (5% weight) at room temperature, upon excitation in the low-lying absorption region (λ: 320–350 nm), compounds **1** and **2** display a bright phosphorescent emission with maxima in the blue region (λ_{max} ~ 450 nm) (see Table 7, Fig. 5 left for **2** and Fig. S8 for **1**). The structured shape of these emission bands, with vibrational spacings [1200 - 1500 cm^{-1}] corresponding to the C=C/C=N stretches of the cyclometalated NHC ligand (C^C*), suggests the involvement of them in their excited state. On the light of their spectral profiles, the absence of significant rigidochromism on going from 298 to 77 K [53], and the theoretical calculations, these emissions can be assigned mainly to a ^{3}IL [π(NHC) → π*(NHC)] excited states This assignment is as well in agreement with the large *singlet-triplet splitting* values [53,54] observed for this complexes (Exp. CH_2Cl_2 77 K, $\Delta E_{S\text{-}T} = 0.69$ eV **1**, 0.68 eV **2**; calculated $\Delta E_{S\text{-}T} = 0.65$ eV **2,** see Fig. S9). Phosphorescence from ligand centered excited states has been also reported for blue-emitting compounds such as (n-Bu_4N)[Pt(4,6-dFppy)$(CN)_2$] [3], or [Pt(C^C)(acac)] [33,54]. However the measured emission lifetimes and theoretical calculations suggest some ^{3}MLCT [5d(Pt) → π*(NHC)] character of the emission, in line with the closely related compounds, $NBu_4[Pt(CN)_2(NHC)]$ (H_2NHC = 1-methyl-3-phenyl-1*H*-imidazolium and 1-methyl-3-phenyl-1*H*-benzimidazolim [11]. The absence of low-energy ^{3}MMLCT [dσ*(Pt)$_2$ → π*(L)] and/or ^{3}ππ* excimeric emission bands prove once more the key role of the counterion size on the emission properties of mononuclear Pt(II) complexes.

Compound **1** rendered moderate photoluminescent quantum

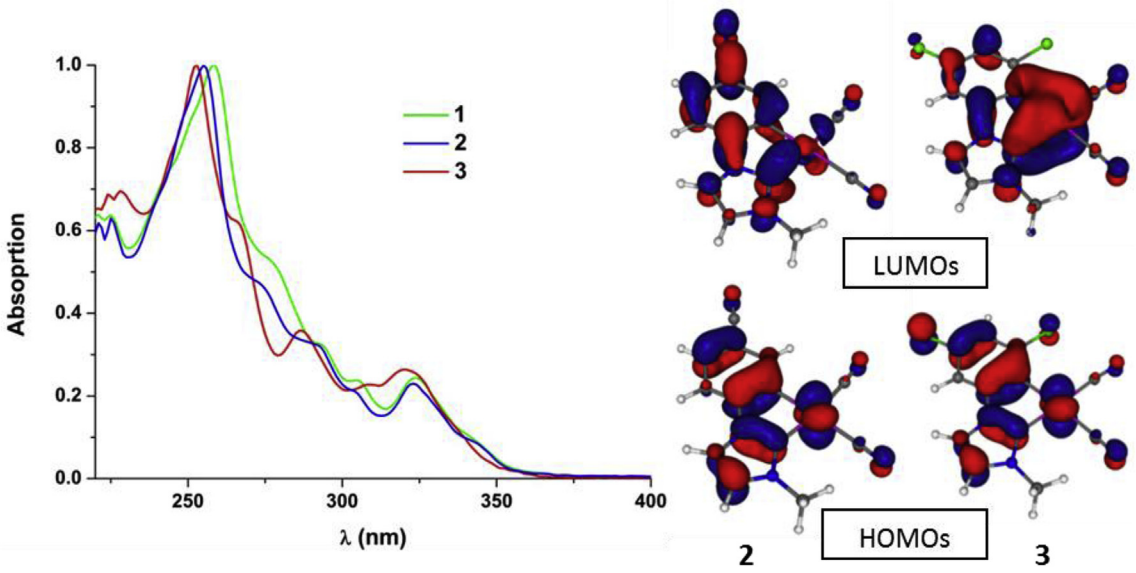

Fig. 4. Absorption spectra of compounds **1**–**3** in CH_2Cl_2 (10^{-4} M) (left). FOs of compounds **2** and **3** calculated in CH_2Cl_2 solution (right).

Table 5
Energy and Population Analysis (%) of Frontier MOs in the Ground State for **2** and **3** in solution of CH_2Cl_2.

MO	eV		Pt		C*		R-C		CN	
	2	3	2	3	2	3	2	3	2	3
L+1	−0.42	−0.32	20	5	13	14	60	79	7	2
L	−1.32	−1.06	14	26	25	31	56	34	5	9
H	−5.71	−5.69	32	30	23	20	40	44	6	5
H-1	−6.08	−6.02	45	37	24	22	17	29	14	12
H-2	−6.09	−6.01	96	97	0	1	2	1	2	1

Table 6
Selected singlet excited states calculated by TD-DFT for **2** and **3**[a].

States	λ_{exc} (calc.)/nm	o.s.	Transition (% contribution)[b]	Assignment
$[Pt(C^{\wedge}C^{*B})(CN)_2]^-$ (2)				
S1	342.50	0.0031	H → L (95%)	^{1}ILCT/^{1}MLCT
S2	315.56	0.0275	H-2 → L (98%)	
S3	303.06	0.1746	H-1 → L (94%)	
$[Pt(C^{\wedge}C^{*C})(CN)_2]^-$ (3)				
S1	327.33	0.0133	H → L (97%)	^{1}ILCT
S2	298.98	0.0431	H-2 → L (99%)	
S3	293.42	0.1705	H-1 → L (92%)	

[a] In solution of CH_2Cl_2.
[b] Transitions with contributions < 10% were not included.

yield (PLQY,Φ) at room temperature, both as neat powder (27%) and in PMMA film (17%), while compound **2** exhibits a more efficient emission (Φ = 62% as powder, 70% in PMMA film).

The CIE coordinates for **1** and **2** are represented in Fig. 5 right, being those for **2** (0.15, 0.19) highly close to the optimal ones for blue emitters (0.15, 0.15) [55]. The calculated radiative rate constants ($k_r = \Phi_{PL}/\tau$) at r.t. were in the order of 10^4 s^{-1} for complex **1** and 10^5 s^{-1} for **2**. This difference suggests a higher IL character in the emission of **1** [3,11] and a more efficient spin-orbit coupling (SOC) for **2**, the latter likely due to a higher contribution of the Pt $6p_z$ orbital to the LUMO [11].

The moderate-good PLQYs, in solid state at r.t., are possible because of the moderate nonradiative rate constants ($k_{nr} = 1/\tau - \Phi_{PL}/\tau$) of ~$10^5$ s^{-1} for **1** and ~10^4 s^{-1} **2**). Since non-radiative deactivation seems unlikely because of the large energy gap between T_1 and S_0 (ca. 22000 cm-1), according to the energy gap law [3], and the insignificant geometrical distortion of T_1 from S_0 (Fig. S10, Table S4), the k_{nr} values suggest the existence of thermal access to dd* states at room temperature, especially for compound **1** [56,57].

In spite of the strong field ligands bonded to platinum, the PLQYs of compounds **1** and **2** in PMMA films at r.t. are lower than the reported ones for [Pt(C^C*)(acac)] (Φ = 0.8–0.98) [33–36,38,51,58], [Pt(C^X-L^L′)] [C^X = phenyl methyl imidazole; L^L′ = carbazolyl pyridine, Φ = 0.89; C^X = phenyl pyrazole; L^L′ = carbazolyl pyridine, Φ = 0.85] [55], or $[Pt(C^{\wedge}C^{*A})(RpzH)_2]A$ (A: ClO_4, PF_6, Rpz: 3,5-dmpz, 4-Mepz, Φ ~ 1) [29]. For powder samples, the PLQYs at r.t. are very similar to the recently published by Kato et al., for $NBu_4[Pt(CN)_2(NHC)]$ (H_2NHC = 1-methyl-3-phenyl-1*H*-imidazolium and 1-methyl-3-phenyl-1*H*-benzimidazolim [11].

The photoluminescent properties of these complexes seem to be strongly affected by the different substituents on the cyclometalated fragment. Then, compound **3** resulted to be emissive just at 77 K (see Table 7). It exhibits a structured emission, ^{3}IL [π(NHC) → π*(NHC)] in nature, as much in rigid matrix of CH_2Cl_2 as in the solid state on the light of its spectrum profile (see Fig. S11) and the theoretical calculations. The absence of luminescence at room temperature could be explained by the existence of thermally accessible higher lying nonradiative dd* excited states and additionally, to the large distortion of the T_1 from the S_0 state (see Fig. S10 and Tables S3 and S5), which enlarge the temperature-independent nonradiative decay rate constant [56,57].

The emission bands of compounds $NBu_4[Pt(C^{\wedge}C^{*A/B/C})(CN)_2]$ in rigid matrix of CH_2Cl_2 appear shifted to higher energies with respect to those of $NBu_4[Pt(C^{\wedge}N)(CN)_2]$(C^N = bzq, ppy) [13], which highlight the effect of the cyclometalated group on them (Fig. 6).

The analysis of the composition and energy of the FOs (HOMO and LUMO) for these compounds agree with the experimental data. The presence of the electron withdrawing groups in the metalated fragment lowers the energy of the HOMO but the carbenic fragment raises more the energy of the LUMO in the C^C* derivatives with respect to those in the C^N ones (see Table S6 in SI), enlarging their HOMO LUMO gap and then shifting their emission to the blue region of the visible spectrum.

The blue-shift of the emissions of these C^C* compounds with respect to $NBu_4[Pt(ppy)(CN)_2]$ is even bigger than the one got in $(NBu_4)[Pt(4,6\text{-dFppy})(CN)_2]$ (4,6-dFppy = 4′,6′-difluorophenyl)

Table 7
Emission data for complexes 1, 2 and 3.

	Medium (T/K)	λ_{ex} (nm)	λ_{em} (nm)	τ (μs)[b]	ϕ	$K_r(s^{-1})$	$K_{nr}(s^{-1})$
1	PMMA[a] (298)	340	448, 474$_{max}$, 505	6.1	0.17	2.8×10^4	1.4×10^5
	Solid (298)	350	454, 478$_{max}$, 507, 537$_{sh}$	6.4	0.27	4.2×10^4	1.1×10^5
	Solid (77)	350	449, 478$_{max}$, 510, 539$_{sh}$	10.8			
	CH_2Cl_2[c](77)	350	448$_{max}$, 478, 512, 543$_{sh}$	15.7			
2	PMMA[a] (298)	330	444, 472$_{max}$, 500, 536$_{sh}$	6.1	0.70	1.1×10^5	4.9×10^4
	Solid (298)	340	446, 471$_{max}$, 501, 530$_{sh}$	6.0	0.62	1.0×10^5	6.3×10^4
	Solid (77)	340	442, 471$_{max}$, 501, 530$_{sh}$	16.0			
	CH_2Cl_2[c] (77)	340	445$_{max}$, 475, 509, 535$_{sh}$	19.9			
3	Solid (77)	340	430$_{max}$, 457, 486, 515$_{sh}$	10.6			
	CH_2Cl_2[c] (77)	340	430$_{max}$, 458, 486, 515$_{sh}$	10.0			

[a] = 5% w/w;
[b] = measured at the λ_{max};
[c] = 10^{-3} M; same results were found at 10^{-5} M.

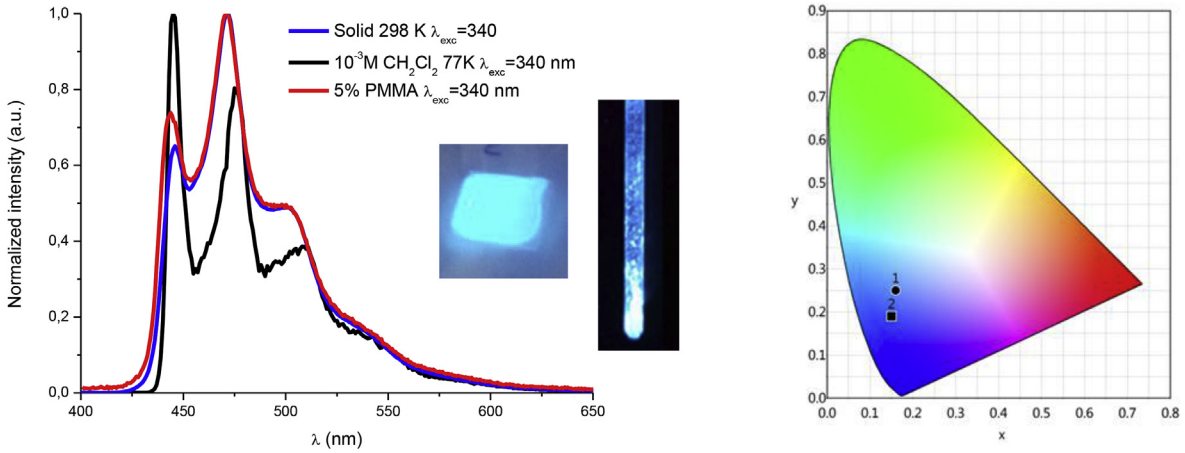

Fig. 5. Normalized emission spectra of **2** (left); Pictures taken for a PMMA film and a powdered sample of **2** under UV light (365 nm). CIE 1931 diagram with the (x, y) positions of the emissions of **1** and **2** in PMMA films (right).

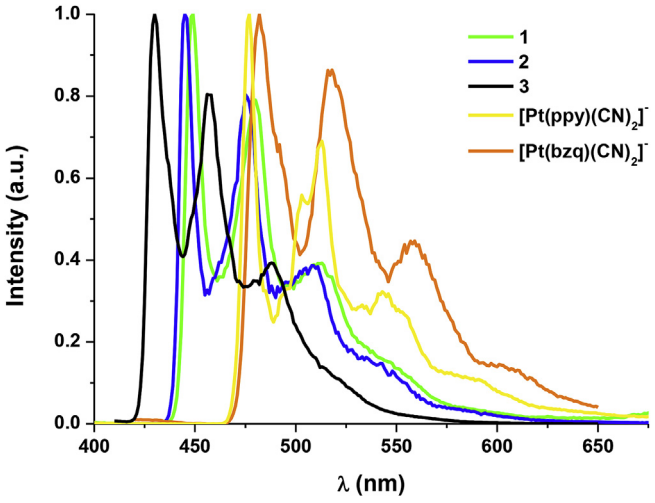

Fig. 6. Normalized emission spectra in CH_2Cl_2 at 77 K.

pyridinate) (λem = 459 nm in neat power) in which the electron withdrawing fluorine atoms attached in the 4 and 6 position stabilize the HOMO with respect to the non-fluorinated ppy [3].

4. Conclusions

In this paper we reported the synthesis, characterization and emissive properties of new anionic platinum (II) complexes containing strong field ligands such as cyclometalated *N*-heterocyclic carbenes and cyanides: $NBu_4[Pt(C^{\wedge}C^{*A/B/C})(CN)_2]$. The upfield shift of the $^{195}Pt\{^1H\}$ NMR signals of **1**–**3** with respect to those of the cyclometalated compounds $NBu_4[Pt(C^{\wedge}N)(CN)_2]$ ($C^{\wedge}N$ = ppy, bzq), and the NBO charge distributions analysis confirmed the bigger donor ability of $C^{\wedge}C^*$ with respect to $C^{\wedge}N$. In their crystal structures, the bulky cations (NBu_4^+) appear intercalated between each two layers of complexes, then avoiding π···π and Pt···Pt interactions among them. This fact has an evident effect on the photoluminescent properties of these compounds, since in rigid media their emissions come from excited states corresponding to isolated molecules, mainly ^{3}IL [π(NHC) → π*(NHC)] in nature, with some little ^{3}MLCT [5d(Pt) → π*(NHC)] character in complexes **1** and **2**.

The analysis of the composition and energy of the FOs (HOMO and LUMO) showed that in these $C^{\wedge}C^*$ derivatives the HOMO is stabilized but the LUMO is destabilized to a larger extent with respect to the FOs of the analogous $C^{\wedge}N$ complexes. As result, their HOMO LUMO gap is larger and their emission is shifted to the blue region of the visible spectrum with respect to them.

The luminescent properties of the reported new compounds are strongly affected by the substituent on the cyclometalated fragment, R = CO_2Et, CN or Cl. In this sense, compound **2** (R = CN) shows the most efficient emission with Φ of 70% in PMMA film and CIE coordinates of (0.15, 0.19), highly close to the optimal ones for blue emitters.

Acknowledgements

This work was supported by the Spanish Ministerio de Economía y Competitividad (MINECO)/FEDER (Project CTQ2015-67461-P led by Dr. Babil Menjón) and by the Gobierno de Aragón and Fondo Social Europeo (Group E17_17R: Química Inorgánica y de los Compuestos Organometálicos led by Dr. José M. Casas). A. C. acknowledges the support of a FPI grant from the Spanish government. The authors thank the Centro de Supercomputación de Galicia (CESGA) for generous allocation of computational resources.

Appendix A. Supplementary data

Supplementary data to this article can be found online at https://doi.org/10.1016/j.jorganchem.2019.03.012.

References

[1] R. Boncarsi, C. Petronglo, E. Scrocco, J. Tomasi, J. Chem. Phys. 48 (1968) 1500.
[2] D.F. Shriver, P.W. Atkins, Inorganic Chemistry, third ed., Oxford University Press, Oxford, 1999.
[3] A.F. Rausch, U.V. Monkowius, M. Zabel, H. Yersin, Inorg. Chem. 49 (2010) 7818–7825.
[4] J. Fornies, V. Sicilia, P. Borja, J.M. Casas, A. Diez, E. Lalinde, C. Larraz, A. Martin, M.T. Moreno, Chem. Asian J. 7 (2012) 2813–2823.
[5] T. Ogawa, M. Yoshida, H. Ohara, A. Kobayashi, M. Kato, Chem. Commun. 51 (2015) 13377–13380.
[6] M. Miskowski, V.H. Houlding, Inorg. Chem. 30 (1991) 4446–4452.
[7] S. Kishi, M. Kato, Mol. Cryst. Liq. Cryst. 379 (2002) 303–308.
[8] M. Kato, K. Sasano, C. Kosuge, M. Yamazaki, S. Yano, M. Kimura, Inorg. Chem. 35 (1996) 116–123.
[9] M. Kato, C. Kosuge, K. Morii, J.S. Ahn, H. Kitagawa, T. Mitani, M. Matsushita, T. Kato, S. Yano, M. Kimura, Inorg. Chem. 38 (1999) 1638–1641.
[10] W.B. Connick, R.E. Marsh, W.P. Schaefer, H.B. Gray, Inorg. Chem. 36 (1997) 913–922.
[11] T. Ogawa, W.M.C. Sameera, D. Saito, M. Yoshida, A. Kobayashi, M. Kato, Inorg. Chem. 57 (2018) 14086–14096.
[12] T. Ogawa, W.M.C. Sameera, M. Yoshida, A. Kobayashi, M. Kato, Dalton Trans. 47 (2018) 5589–5594.
[13] J. Forniés, S. Fuertes, J.A. López, A. Martín, V. Sicilia, Inorg. Chem. 47 (2008) 7166–7176.
[14] S.M. Drew, D.E. Janzen, C.E. Buss, D.I. MacEwan, K.M. Dublín, K.R. Mann, J. Am. Chem. Soc. 123 (2001) 8414–8415.
[15] S.M. Drew, D.E. Janzen, K.R. Mann, Anal. Chem. 74 (2002) 2547–2555.
[16] S.M. Drew, J.E. Mann, B.J. Marquardt, K.R. Mann, Sens. Actuators, B 97 (2004) 307–312.
[17] C.E. Buss, C.E. Anderson, M.K. Pomije, C.M. Lutz, D. Britton, K.R. Mann, J. Am. Chem. Soc. 120 (1998) 7783–7790.
[18] B.M. Anderson, S.K. Hurst, Eur. J. Inorg. Chem. (2009) 3041–3054.
[19] G. Aullón, S. Alvarez, Chem. Eur J. 3 (1997) 655–664.
[20] J.P.H. Charmant, J. Forniés, J. Gómez, E. Lalinde, R.I. Merino, M.T. Moreno, G. Orpen, Organometallics 18 (1999) 3353–3358.
[21] S.M. Drew, L.I. Smith, K.A. McGee, K.R. Mann, Chem. Mater. 21 (2009) 3117–3124.
[22] C.E. Buss, K.R. Mann, J. Am. Chem. Soc. 124 (2002) 1031–1039.
[23] A.G. Dylla, D.E. Janzen, M.K. Pomije, K.R. Mann, Organometallics 26 (2007) 6243–6247.
[24] Y. Sun, K. Ye, H. Zhang, J. Zhang, L. Zhao, B. Li, G. Yang, B. Yang, Y. Wang, S.W. Lai, C.M. Che, Angew. Chem. Int. Ed. 45 (2006) 5610–5613.
[25] I. Eryazici, C.N. Moorefield, G.R. Newkome, Chem. Rev. 108 (2008) 1834–1895.
[26] S.Y.L. Leung, A.Y.Y. Tam, C.H. Tao, H.S. Chow, V.W.W. Yam, J. Am. Chem. Soc. 134 (2012) 1047–1056.
[27] M. Kato, Bull. Chem. Soc. Jpn. 80 (2007) 287–294.
[28] V.W.W. Yam, V.K.M. Au, S.Y.-L. Leung, Chem. Rev. 115 (2015) 7589–7728.
[29] L. Arnal, S. Fuertes, A. Martin, V. Sicilia, Chem. Eur J. 24 (2018) 9377–9384.
[30] S. Fuertes, A.J. Chueca, L. Arnal, A. Martín, U. Giovanella, C. Botta, V. Sicilia, Inorg. Chem. 56 (2017) 4829–4839.
[31] S.-B. Ko, H.-J. Park, S. Gong, X.N. Wang, Z.-H. Lu, S.N. Wang, Dalton Trans. 44 (2015) 8433–8443.
[32] A. Tronnier, S. Metz, G. Wagenblast, I. Münster, T. Strassner, Dalton Trans. 43 (2014) 3297–3305.
[33] Y. Unger, D. Meyer, O. Molt, C. Schildknecht, I. Münster, G. Wagenblast, T. Strassner, Angew. Chem. Int. Ed. 49 (2010) 10214–10216.
[34] A. Tronnier, G. Wagenblast, I. Münster, T. Strassner, Chem. Eur J. 21 (2015) 12881–12884.
[35] M. Tenne, S. Metz, G. Wagenblast, I. Münsterb, T. Strassner, Dalton Trans. 44 (2015) 8444–8455.
[36] J. Soellner, T. Strassner, Organometallics 37 (2018) 1821–1824.
[37] P. Pinter, Y. Unger, T. Strassner, ChemPhotoChem 1 (2017) 113–115.
[38] Z.M. Hudson, C. Sun, M.G. Helander, Y.L. Chang, Z.H. Lu, S.N. Wang, J. Am. Chem. Soc. 134 (2012) 13930–13933.
[39] V. Sicilia, S. Fuertes, A.J. Chueca, L. Arnal, A. Martin, M. Perálvarez, C. Botta, U. Giovanella, J. Mater. Chem. (2019), https://doi.org/10.1039/C1039TC00747D. C., In Press.
[40] T. Fleetham, g. Li, J. Li, Adv. Mater. 29 (2017), 1601861.
[41] C. RED, CCD Camera Data Reduction Program, Oxford Diffraction, Oxford, UK, 2004.
[42] G.M. Sheldrick, Acta Crystallogr. A 64 (2008) 112–122.
[43] L. Farrugia, J. Appl. Crystallogr. 32 (1999) 837–838.
[44] Y. Zhao, D.G. Truhlar, Theor.Chem. Acc. 120 (2008) 215–241.
[45] M.J. Frisch, G.W. Trucks, H.B. Schlegel, G.E. Scuseria, M.A. Robb, J.R. Cheeseman, G. Scalmani, V. Barone, B. Mennucci, G.A. Petersson, H. Nakatsuji, M. Caricato, X. Li, H.P. Hratchian, A.F. Izmaylov, J. Bloino, G. Zheng, J.L. Sonnenberg, M. Hada, M. Ehara, K. Toyota, R. Fukuda, J. Hasegawa, M. Ishida, T. Nakajima, Y. Honda, O. Kitao, H. Nakai, T. Vreven, J.A. Montgomery Jr., J.E. Peralta, F. Ogliaro, M.J. Bearpark, J. Heyd, E.N. Brothers, K.N. Kudin, V.N. Staroverov, R. Kobayashi, J. Normand, K. Raghavachari, A.P. Rendell, J.C. Burant, S.S. Iyengar, J. Tomasi, M. Cossi, N. Rega, N.J. Millam, M. Klene, J.E. Knox, J.B. Cross, V. Bakken, C. Adamo, J. Jaramillo, R. Gomperts, R.E. Stratmann, O. Yazyev, A.J. Austin, R. Cammi, C. Pomelli, J.W. Ochterski, R.L. Martin, K. Morokuma, V.G. Zakrzewski, G.A. Voth, P. Salvador, J.J. Dannenberg, S. Dapprich, A.D. Daniels, Ö. Farkas, J.B. Foresman, J.V. Ortiz, J. Cioslowski, D.J. Fox, Gaussian, Inc., Wallingford, CT, USA, 2009.
[46] D. Andrae, U. Häußermann, M. Dolg, H. Stoll, H. Preuß, Theor. Chim. Acta 77 (1990) 123–141.
[47] R. Ditchfield, W.J. Hehre, J.A. Pople, J. Chem. Phys. 54 (1971) 724–728.
[48] P.C. Hariharan, J.A. Pople, Theor. Chim. Acta 28 (1973) 213–222.
[49] J. Fornies, S. Fuertes, C. Larraz, A. Martín, V. Sicilia, A.C. Tsipis, Organometallics 31 (2012) 2729–2740.
[50] S. Fuertes, A.J. Chueca, V. Sicilia, Inorg. Chem. 54 (2015) 9885–9895.
[51] T. Strassner, Acc. Chem. Res. 49 (2016) 2680–2689.
[52] S. Fuertes, A.J. Chueca, M. Perálvarez, P. Borja, M. Torrell, J. Carreras, V. Sicilia, ACS Appl. Mater. Interfaces 8 (2016) 16160–16169.
[53] A. Tsuboyama, H. Iwawaki, M. Furugori, T. Mukaide, J. Kamatani, S. Igawa, T. Moriyama, S. Miura, T. Takiguchi, S. Okada, M. Hoshino, K. Ueno, J. Am. Chem. Soc. 125 (2003) 12971–12979.
[54] S. Haneder, E. Da Como, J. Feldmann, J.M. Lupton, C. Lennartz, P. Erk, E. Fuchs, O. Molt, I. Münster, C. Schildknecht, G. Wagenblast, Adv. Mater. 20 (2008) 3325–3330.
[55] T. Fleetham, Z.X. Wang, J. Li, Org. Electron. 13 (2012) 1430–1435.
[56] Y. Luo, Y. Xu, W. Zhang, W. Li, M. Li, R. He, W. Shen, J. Phys. Chem. C 120 (2016) 3462–3471.
[57] Y. Luo, Z. Chen, J. Zhang, Y. Tang, Z. Xu, D. Tang, RSC Adv. 6 (2016) 113513–113521.
[58] S. Fuertes, A.J. Chueca, A. Martin, V. Sicilia, Cryst. Growth Des. 17 (2017) 4336–4346.